

Control of a Single-Switch Two-Input Buck Converter for MPPT of Two PV Strings

Andoni Urtasun, *Student Member, IEEE*, Dylan Dah-Chuan Lu, *Senior Member, IEEE*

Abstract—In this paper, the Two-Input Buck (TIBuck) converter is proposed as the DC/DC stage for photovoltaic (PV) cascaded converters. This converter is attractive for this application because it is cost-effective and reliable and can achieve dual maximum power point tracking (MPPT) with only one power transistor. However, due to the simplified and integrated structure, the nonlinear characteristics of the converter and the two PV arrays complicate the control. By means of a small-signal modeling, the control theme of the two PV voltages is formulated and the effect of the nonlinearities is presented. It is shown that, while fast voltage dynamics are achieved for the first input, the second-input voltage response depends on the second-stage converter control. Simulation and experimental results are reported to validate the theoretical analysis, showing the dual MPPT capability.

Index Terms—Dual MPPT, Photovoltaic power systems, Small-signal modeling, Two-input converters, Voltage control.

I. INTRODUCTION

Photovoltaic systems are experiencing continuous expansion and development, particularly in grid-connected applications. More than 39 GW were added during 2013, bringing worldwide total capacity to approximately 139 GW. Almost half of all PV capacity in operation was added in the past two years, and 98% has been installed since the beginning of 2004 [1].

In order to process the photovoltaic energy, electronic converters are generally required. For this purpose, it is usual to use cascaded converters, where the first stage is a DC/DC converter and, in case of grid-connected PV systems or stand-alone PV systems with AC loads, the second stage is a DC/AC inverter. A simple and reliable solution for the first stage is to install conventional DC/DC converters such as the buck, boost or buck/boost, as shown in Fig. 1(a) [2]–[4]. These configurations are attractive from a component count perspective but only perform one MPPT algorithm per converter. However, given that different PV module technologies, orientations and shading conditions are common in many applications, these converters can result in significant power losses [5]–[8].

Manuscript received December 15, 2014; revised March 12, 2015; accepted April 8, 2015.

Copyright (c) 2015 IEEE. Personal use of this material is permitted. However, permission to use this material for any other purposes must be obtained from the IEEE by sending a request to pubs-permissions@ieee.org.

This work was supported in part by the Public University of Navarra through a doctoral scholarship.

A. Urtasun is with the Department of Electrical and Electronic Engineering, Public University of Navarra, Pamplona, Spain (e-mail: andoni.urtasun@unavarra.es).

D. D.-C. Lu is with the School of Electrical and Information Engineering, University of Sydney, Sydney, NSW 2006, Australia (e-mail: dylan.lu@sydney.edu.au).

In order to reduce the effects of mismatch on the power production of the PV generator, various solutions have been proposed. A review of a number of alternatives is carried in [9], where the different actions are divided into three groups: modifying the MPPT algorithm [10], [11], changing the electrical connection of the panels into the PV field [12], and modifying the power electronics system architecture [13], [14]. Within the latter group, a frequently adopted solution is to place an arbitrary number of n DC/DC converters in parallel, as shown in Fig. 1(b) [15]–[18]. Although the conversion efficiency is lower when compared to the previous configurations, it makes it possible to perform n independent MPPTs. As a result, the overall efficiency is higher for applications under different shading conditions, orientations or module technologies.

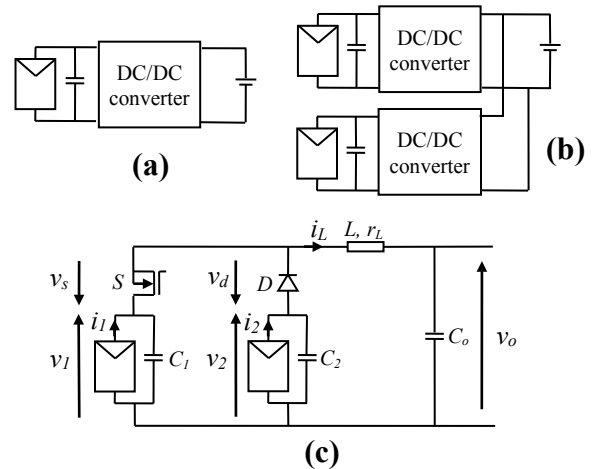


Fig. 1. Configurations for the DC/DC stage of PV systems: (a) Single DC/DC converter, (b) Multiple DC/DC converters, (c) Proposed scheme.

As an alternative to n single-input converters, n -input DC/DC converters have been proposed in the literature, where the case $n=2$ is the most frequently analyzed [19]–[26]. These converters aim to improve the system performance in terms of conversion efficiency, integration and cost, while, at the same time, maintain the dual MPPT capability. However, most of the proposed converters still use more than one active switch and several passive components, limiting them from achieving higher power density or higher efficiency.

This paper proposes the Two-Input Buck (TIBuck) converter as the DC/DC stage for PV systems, as shown in Fig. 1(c). Similarly to the previous cases, this configuration also achieves two MPPTs. However, only one power transistor is required for the DC/DC conversion, making the system more cost-effective and reliable. Furthermore, given the low switch and diode voltage stress and the low voltage variation

across the inductor, the TIBuck efficiency can reach high values (up to 99.7%) and a small inductance is required [27].

The TIBuck converter was first proposed by Sebastian *et al.* in [27] to improve AC/DC conversion efficiency. In this first application, the output voltage was the control variable. Based on the efficient converter structure, this paper, however, focuses on the ability of the converter to achieve dual MPPT and dual voltage regulation under different control conditions. The nonlinearity of the two PV arrays must be considered, which adds complexity to the analysis of the nonlinear converter [28]–[31]. Small-signal modeling is carried out in order to apply linear control techniques.

The control proposed in this paper thus considers that the cascaded system is connected to an AC voltage source. This assumption is valid for grid-connected applications as well as stand-alone systems in which the grid voltage is generated by another element, such as a battery inverter or a diesel generator [32]. Depending on the PV and grid voltages and whether an isolation transformer is required, a step-up or step-down inverter should be used as the second-stage converter.

The paper is organized as follows. In Section II, the control scheme for the proposed configuration is presented. The small-signal model is then derived in Section III. The regulation of both input voltages is presented in Section IV. In Section V, simulation results are provided to verify the control performance. Then, section VI reports experimental validation of the small-signal model and the voltage regulations. In Section VII, an extension of the two-input buck converter, a multiple-input buck converter, is briefly introduced. Finally, conclusions of this work are given in Section VIII.

II. DUAL MPPT WITH TIBUCK CONVERTER

The TIBuck is shown in Fig. 1(c), where i_1 and i_2 are the PV currents, v_1 and v_2 the PV voltages, v_o the output voltage, v_s the switch voltage, v_d the diode voltage, and i_L the inductor current. This converter is similar to the conventional buck converter, excluding that a second input is added. Two capacitors, C_1 and C_2 , are placed in parallel with the two PV strings, respectively, to change the causality from current source to voltage source and reduce the voltage ripple.

The elements used throughout the paper are presented in Table I and II. Table I shows the features of the TIBuck converter. According to [33], the capacitor values have been chosen so that the MPPT losses due to the voltage ripple are lower than 0.2%. The inductor value is obtained in order to avoid discontinuous conduction mode operation and limit the current ripple. Table II shows the specifications of the PV arrays, where the parameters are given for the series-connected configurations. The TIBuck converter makes it possible to interface with different types of PV modules in its two inputs, with the only restriction that v_1 must be greater than v_2 . To show this benefit, the results are provided for three series-connected polycrystalline modules at input 1 (PV1) and two series-connected monocrystalline modules at input 2 (PV2).

Due to the second input, the voltage across the switches is $v_1 - v_2$ for the TIBuck converter, much lower than for the buck converter. As a result, the TIBuck converter is more reliable and its efficiency is higher. Indeed, its maximum efficiency was shown to be 99.7% for high input voltages, and 97.6% for low input voltages, already in the year 1998 [27]. Although

this paper is focused on the control rather than the efficiency, the TIBuck efficiency has been estimated as 98.7% for low input voltages: $V_1=52$ V, $V_2=36$ V, $P_o=400$ W, power MOSFET STL11N4LLF5 ($V_{Smax}=40$ V) and power Schottky diode STPS1045DEE ($V_{Smax}=45$ V). For this estimation, MOSFET, diode, inductor and capacitor losses have been calculated at the mentioned operating point.

The control scheme is shown in Fig. 2. The MPPT algorithm requires the duty cycle reference d_{ref} as well as the measured variables $v_{1,m}$, $v_{2,m}$, and $i_{L,m}$ as inputs. With this information, the algorithm provides the reference voltages $v_{1,ref}$ and $v_{2,ref}$ to be controlled. The way of obtaining these references depends on the MPPT technique. To illustrate the process, a brief example is provided for the perturbation and observation (P&O) algorithm. The P&O first changes $v_{1,ref}$ and $v_{2,ref}$ and waits until the steady-state is reached. At that moment, the PV1 power is obtained as $P_{pv1} = V_1 \cdot D \cdot I_L$, where D is the steady-state duty cycle, and, depending on the power variation, the algorithm decides if increase, maintain or decrease $v_{1,ref}$. Simultaneously, the PV2 power is determined as $P_{pv2} = V_2 \cdot (1-D) \cdot I_L$, and the same decision is made in relation to $v_{2,ref}$. The $v_{1,ref}$ and $v_{2,ref}$ variations are applied at the same time as voltage steps and their magnitude depend on the P&O algorithm. More details about MPPT algorithms can be consulted in [34] and [35]. In other situations, the PV power does not have to be maximized but needs to be limited [36]. In any case, this paper deals with the fundamental requirement of voltage regulation of the proposed converter architecture, whether it is applied to MPPT algorithm or power limitation. It is thus assumed that the reference voltages are known.

TABLE I
FEATURES OF THE TIBUCK CONVERTER

Rated power	400 W
Input capacitor C_1	32 μ F
Input capacitor C_2	32 μ F
Inductor L	44 μ H
Commutation frequency f	50 kHz

TABLE II
SPECIFICATIONS OF THE PV ARRAYS

PV1 module model	Sharp NE-080T1J
PV1 array MPP power P_{MPP1}	240 W
PV1 array MPP voltage V_{MPP1}	51.9 V
PV1 array MPP current I_{MPP1}	4.63 A
PV1 array open-circuit voltage V_{oc1}	64.8 V
PV1 array short-circuit current I_{SC1}	5.15 A
PV2 module model	Hurricane HS-80D
PV2 array MPP power P_{MPP2}	160 W
PV2 array MPP voltage V_{MPP2}	36 V
PV2 array MPP current I_{MPP2}	4.5 A
PV2 array open-circuit voltage V_{oc2}	44 V
PV2 array short-circuit current I_{SC2}	4.7 A

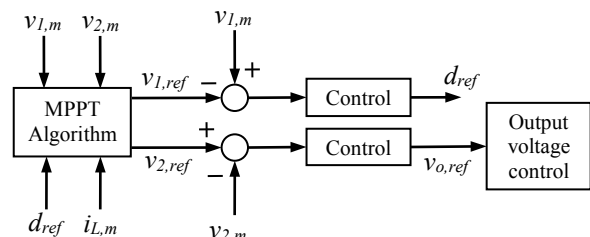


Fig. 2. Control scheme for dual MPPT with TIBuck converter.

The two input voltages can be controlled by the two degrees of freedom, namely the TIBuck switch commutation and the output voltage v_o . From the PV1 voltage error, the control obtains the switch duty cycle reference, d_{ref} , from which the switch commutations are found after the modulation. From the PV2 voltage error, the other control obtains the output voltage reference, $v_{o,ref}$. In turn, this voltage is then regulated by the second-stage converter. As a result of this inner voltage control and depending on the second-stage converter, the PV2 voltage regulation is dynamically restricted, as it will be shown later. On the other hand, the proposed control requires the output voltage v_o to be variable, which could impact on the efficiency of the second stage converter. For this reason, the authors recommend the use of converters whose efficiency is insensitive to input voltage variation around the rated value. There are a number of converters with these features and different input voltage ranges. Two examples are presented in [37] and [38], where the inverters are capable of a 50% voltage variation with less than 0.5% reduction in efficiency in relation to the most efficient operating point.

III. SMALL-SIGNAL MODELING

Since the output voltage is controlled by the inverter, it will be considered as a controlled voltage source. It is also assumed that the TIBuck converter is operating in continuous conduction mode. In this mode, the switch is conducting and the diode is off for $u=1$, while the switch is off and the diode is conducting for $u=0$, where u is the commutation function. Considering the switch, diode and inductor losses in the model is important for the design of the PV1 voltage control, as it will be shown in section IV.A. Applying Kirchhoff's laws to the system which is presented in Fig. 1(c), and considering average values, one obtains

$$C_1 \cdot \frac{dv_1}{dt} = i_1 - d \cdot i_L \quad (1)$$

$$C_2 \cdot \frac{dv_2}{dt} = i_2 - (1-d) \cdot i_L \quad (2)$$

$$L \cdot \frac{di_L}{dt} = d \cdot (v_1 - v_{s,on}) + (1-d) \cdot (v_2 - v_{d,on}) - r_L \cdot i_L - v_o, \quad (3)$$

where d is the TIBuck switch duty cycle, $v_{s,on}$ is the switch voltage drop during conduction, and $v_{d,on}$ is the diode voltage drop during conduction.

From (1)–(3), the steady-state equations can be worked out as

$$I_1 = D \cdot I_L \quad (4)$$

$$I_2 = (1-D) \cdot I_L \quad (5)$$

$$V_0 = D \cdot (V_1 - V_{s,on}) + (1-D) \cdot (V_2 - V_{d,on}) - r_L \cdot I_L, \quad (6)$$

where steady-state variables are expressed in capital letters.

The converter model represented by (1)–(3) is nonlinear. In order to use linear control techniques, small-signal analysis is applied to those equations, resulting in

$$C_1 \cdot \frac{d\hat{v}_1}{dt} = \hat{i}_1 - D \cdot \hat{i}_L - I_L \cdot \hat{d} \quad (7)$$

$$C_2 \cdot \frac{d\hat{v}_2}{dt} = \hat{i}_2 - (1-D) \cdot \hat{i}_L + I_L \cdot \hat{d} \quad (8)$$

$$L \cdot \frac{d\hat{i}_L}{dt} = D \cdot (\hat{v}_1 - \hat{v}_{s,on}) + (1-D) \cdot (\hat{v}_2 - \hat{v}_{d,on}) - r_L \cdot \hat{i}_L + (V_1 - V_2 - V_{s,on} + V_{d,on}) \cdot \hat{d} - \hat{v}_0 \quad (9)$$

where small-signal variables are marked with a circumflex and the operating point is defined by (4)–(6).

The voltage drop during conduction across the switch and diode can be approximated by a constant voltage source in series with a resistor, namely r_s for the switch and r_d for the diode. As a result, the switch and diode small-signal model can be expressed as

$$\hat{v}_{s,on} = r_s \cdot \hat{i}_L \quad (10)$$

$$\hat{v}_{d,on} = r_d \cdot \hat{i}_L. \quad (11)$$

PV currents i_1 and i_2 depend on the PV voltage, the irradiation and the array temperature through nonlinear expressions. Since the temperature variation is very slow, its small-signal effect can be neglected. The small-signal model for the PV arrays can then be expressed as follows [28]:

$$\hat{i}_1 = K_{g1} \cdot \hat{g}_1 - \frac{\hat{v}_1}{R_1} \quad (12)$$

$$\hat{i}_2 = K_{g2} \cdot \hat{g}_2 - \frac{\hat{v}_2}{R_2}, \quad (13)$$

where \hat{g}_1 and \hat{g}_2 are the small-signal irradiancies, K_{g1} and K_{g2} are the coefficients of the PV current variation with the irradiation, and R_1 and R_2 are the dynamic resistances of the arrays. The dynamic resistance is related to the slope of the I - V curve and represents the PV array nonlinear behavior. In the constant current region, it reaches high values, while in the constant voltage region, it has low values.

Introducing (10)–(13) into (7)–(9), reordering and applying Laplace transforms lead to

$$s \cdot X = A \cdot X + B \cdot U, \quad (14)$$

where

$$X = [\hat{v}_1 \quad \hat{v}_2 \quad \hat{i}_L]^T \quad (15)$$

$$U = [\hat{g}_1 \quad \hat{g}_2 \quad \hat{d} \quad \hat{v}_0]^T \quad (16)$$

$$A = \begin{bmatrix} -1/R_1 C_1 & 0 & -D/C_1 \\ 0 & -1/R_2 C_2 & -(1-D)/C_2 \\ D/L & (1-D)/L & -r_{eq}/L \end{bmatrix} \quad (17)$$

$$B = \begin{bmatrix} K_{g1}/C_1 & 0 & -I_L/C_1 & 0 \\ 0 & K_{g2}/C_2 & I_L/C_2 & 0 \\ 0 & 0 & V_{eq}/L & -1/L \end{bmatrix} \quad (18)$$

$$r_{eq} = D \cdot r_s + (1-D) \cdot r_d + r_L \quad (19)$$

$$V_{eq} = (V_1 - V_{s,on}) - (V_2 - V_{d,on}). \quad (20)$$

IV. VOLTAGE REGULATION

A. Plant for the PV1 Voltage Regulation

The PV1 voltage is regulated by means of the TIBuck switch duty cycle through a single feedback loop. The loop for the PV1 voltage regulation is shown in Fig. 3, where C_{v1} represents the controller, S_{v1} the digital sampler, G_{v1-d} the duty cycle to PV1 voltage transfer function, and H_{v1} the PV1 voltage sensing. As shown in (14), the PV1 voltage also depends on the output voltage v_0 , which is a disturbance for this control. However, since the PV1 voltage control is much faster than the output voltage control, the effect of this disturbance can be neglected.

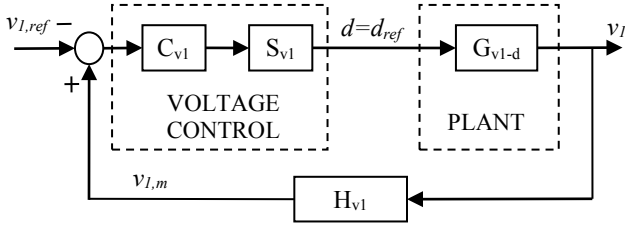


Fig. 3. PV1 voltage control loop.

In order to design the controller, the system plant must be worked out. Transfer function G_{v1-d} can be obtained from (14)–(18), and its expression is as follows:

$$G_{v1-d} = \frac{\hat{v}_1}{\hat{d}} = -\frac{a_2 \cdot s^2 + a_1 \cdot s + a_0}{b_3 \cdot s^3 + b_2 \cdot s^2 + b_1 \cdot s + b_0}, \quad (21)$$

where

$$a_2 = I_L \cdot L \cdot C_2 \quad (22)$$

$$a_1 = I_L \cdot L / R_2 + I_L \cdot r_{eq} \cdot C_2 + D \cdot V_{eq} \cdot C_2 \quad (23)$$

$$a_0 = I_L \cdot r_{eq} / R_2 + I_L \cdot (1-D) + D \cdot V_{eq} / R_2 \quad (24)$$

$$b_3 = L \cdot C_1 \cdot C_2 \quad (25)$$

$$b_2 = L \cdot (C_1 / R_2 + C_2 / R_1) + r_{eq} \cdot C_1 \cdot C_2 \quad (26)$$

$$b_1 = L / (R_1 \cdot R_2) + r_{eq} (C_1 / R_2 + C_2 / R_1) + (1-D)^2 C_1 + D^2 C_2 \quad (27)$$

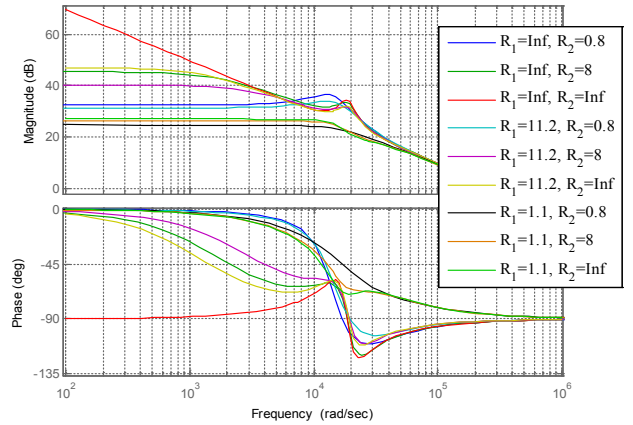
$$b_0 = r_{eq} / (R_1 \cdot R_2) + (1-D)^2 / R_1 + D^2 / R_2. \quad (28)$$

As it can be observed in (21)–(28), the plant zeros and poles are variable depending on the operating point because the converter and the PV arrays are nonlinear. As it has been proved in some papers, the variability of the dynamic resistance diminishes the voltage regulation performance and can compromise the stability for some operating points [28]–[31]. For the proposed configuration, the analysis becomes even more delicate because not only one but two different dynamic resistances take part in the control.

The effect of the two dynamic resistances, R_1 and R_2 , will be analyzed here. In order to ensure stability, the dynamic resistance variation within the whole operating range must be taken into account. For MPP, dynamic resistance can be readily obtained as $R_{MPP} = V_{MPP} / I_{MPP}$, leading to $R_{MPP1} = 11.2 \Omega$ and $R_{MPP2} = 8 \Omega$ in this case [39]. During the system startup or PV power limitation, the system operates in the constant

voltage region. At open-circuit voltage, the dynamic resistance has its smallest value, which can be roughly estimated as $R_{min} = R_{MPP} / 10$. On the other hand, transients can make the system operate at the constant current region, where the dynamic resistance increases very quickly. The value $R_{max} = \infty$ can be used in this case. The operating range $R_{MPP} / 10 < R < \infty$ must therefore be considered. More details about the dynamic resistance variation range can be consulted in [28].

Fig. 4 shows the bode plot of the transfer function $-G_{v1-d}$ for the nine possible combinations of R_{min1} , R_{MPP1} , R_{max1} with R_{min2} , R_{MPP2} , R_{max2} . The large influence of the dynamic resistances on the plant can be observed, especially for low frequencies. Two conjugate poles appear between 14000–19000 rad/s (about 2200–3000 Hz), being less damped for high dynamic resistance values. Besides, these two poles highly depend on the switch, diode and inductor losses, which should not therefore be neglected for the analysis. Then, from a certain frequency, all curves tend to join together and the dynamic resistance effect disappears.


 Fig. 4. Bode plot of $-G_{v1-d}$ for different R_1 and R_2 values.

B. Controller Design for the PV1 Voltage Regulation

According to Fig. 4, the frequency from which the dynamic resistance effect is no longer present is too high for practical purposes. This frequency could be reduced by increasing the capacitor and inductor values, making it possible to achieve high dynamics as well as prevent the dynamic resistance effect. However, a considerable increase is required in the passive components, which increases the size and cost of the solution.

Instead, a crossover frequency f_c below the resonance frequency f_r is chosen. For the controller design, the resistance values $R_1 = R_{max1}$ and $R_2 = R_{max2}$ are considered since the plant bode plot is more problematic concerning stability. In fact, the resonance peak is higher and the phase is lower than for other resistance combinations (see Fig. 4). In order to prevent the resonance peak from cutting the 0 dB axis and ensure a certain Gain Margin (GM), the crossover frequency cannot be close to the resonance one. It is therefore selected as $f_c = 500$ Hz, while $f_r = 3000$ Hz. A pole at $\omega_p = 2\pi \cdot 600$ rad/s is added to the conventional PI controller in order to further enhance the gain margin, and the Phase Margin (PM) is imposed to 40° . The controller C_{v1} is thus a type II amplifier, which has three parameters, namely K_p , T_n and ω_p , and can be expressed as

$$C_{v1} = K_p \frac{T_n \cdot s + 1}{T_n \cdot s} \cdot \frac{\omega_p}{\omega_p + s}. \quad (29)$$

The bode plot of the compensated system is shown in Fig. 5 for three different dynamic resistance combinations. Transfer functions S_{v1} and H_{v1} are modeled as first order low-pass filters with time constants $\tau_s=1.5 \cdot T_S=30 \mu s$ and $\tau_h=26.5 \mu s$, respectively, where T_S is the sample time (see Fig. 3). Since the regulator is designed for $R_1=R_{max1}$ and $R_2=R_{max2}$, it can be observed that the control behaves as desired, that is $f_c=500$ Hz and $PM=40^\circ$. Besides, thanks to the controller pole at $\omega_p=2\pi \cdot 600$ rad/s, the gain margin is high enough, $GM=18$ dB. However, when the system operates with dynamic resistances different from the design values, the voltage response differs. When both PV arrays are operating at MPP, i.e. $R_1=R_{MPP1}$ and $R_2=R_{MPP2}$, it can be seen in the figure how the response becomes slower and more damped, with $f_c=350$ Hz and $PM=103^\circ$. On the other hand, when both PV arrays are at open-circuit, $R_1=R_{min1}$ and $R_2=R_{min2}$, and the effect of the dynamic resistances becomes enormous, slowing down the response to $f_c=12$ Hz, and with $PM=102^\circ$.

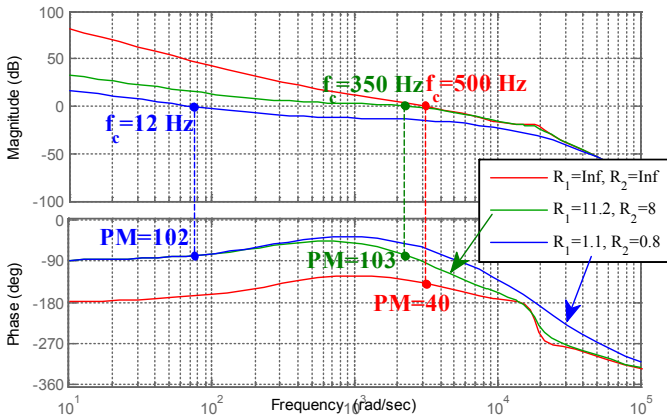


Fig. 5. Bode plot of the compensated system $-C_{v1} \cdot S_{v1} \cdot G_{v1,d} \cdot H_{v1}$.

Fig. 6 shows the effect of the dynamic resistances on the voltage response in more detail. The crossover frequency and the phase margin are represented as a function of R_1 for three different R_2 values ($R_{min2}=0.8 \Omega$, $R_{MPP2}=8 \Omega$ and $R_{max2}=\infty$). It can be clearly observed that, as the dynamic resistances get lower than the maximum values, the phase margin increases. As a consequence, the system is stable for every operating point. Concerning the dynamics, the response slows down when the resistances decrease. However, the voltage response is very quick for every operating point except for the points very close to open-circuit voltage.

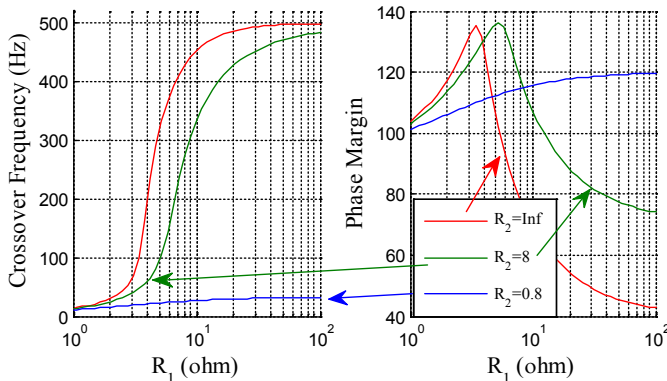


Fig. 6. Crossover frequency and phase margin as a function of R_1 for three different R_2 ($R_{min2}=0.8 \Omega$, $R_{MPP2}=8 \Omega$ and $R_{max2}=\infty$), for PV1 voltage regulation.

C. PV2 Voltage Regulation

The PV2 voltage is regulated through cascaded feedback loops. The outer loop obtains the output voltage reference $v_{0,ref}$, which is controlled by the second stage converter. In case of an grid-connected inverter, this voltage $v_{0,ref}$ is controlled by means of a third loop, which regulates the grid current. The control loop for the PV2 voltage regulation is shown in Fig. 7, where C_{v2} represents the controller, S_{v2} the digital sampler, $G_{v0,cl}$ the output voltage closed-loop, G_{v2-v0} the output voltage to PV2 voltage transfer function, and H_{v2} the PV2 voltage sensing.

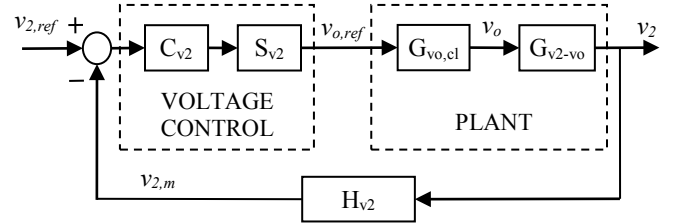


Fig. 7. PV2 voltage control loop.

The dynamics of the output voltage closed-loop depends on the control of the second-stage converter. For example, the crossover frequency for the v_0 regulation is about 20 Hz for a single-phase inverter and about 70 Hz for a three-phase inverter [40]. This supposes a dynamic limitation for the PV2 regulation, which is taken into account by means of the closed-loop transfer function $G_{v0,cl}$. In this paper, the most restrictive case, that is the single-phase inverter, will be considered.

In order to obtain the plant transfer function G_{v2-v0} , it can be considered that the PV1 voltage regulation is instantaneous in relation to the PV2 voltage regulation. This makes it possible not to take the duty cycle into account, but instead to consider the reference voltage $v_{1,ref}$ as an external disturbance. In doing so, G_{v2-v0} can be obtained from the model of section III as

$$G_{v2-v0} = \frac{k}{s^2 / \omega_n^2 + 2 \cdot \xi \cdot s / \omega_n + 1}, \quad (30)$$

where

$$k = \left[r_{eq} / R_2 + D \cdot V_{eq} / (R_2 \cdot I_L) + (1-D) \right]^{-1} \quad (31)$$

$$\omega_n = 1 / \sqrt{k \cdot L \cdot C_2} \quad (32)$$

$$\xi = 1/2 \cdot \sqrt{k / (L \cdot C_2)} \cdot (L / R_2 + r_{eq} \cdot C_2 + D \cdot V_{eq} \cdot C_2 / I_L). \quad (33)$$

From (30), the plant G_{v2-v0} possesses two poles. Since ξ is always higher than zero, both poles are in the left half-plane. Furthermore, because ω_n is much higher than the frequencies of concern for the PV2 voltage regulation, G_{v2-v0} can be approximated as a constant value, that is

$$G_{v2-v0} \approx k. \quad (34)$$

The controller C_{v2} is an integral controller, $C_{v2}=K_i/s$, where K_i is the integral gain, and is designed to obtain a crossover frequency equal to 10 Hz for $R_2 \rightarrow \infty$. However, similarly to the PV1 voltage control, the PV2 voltage regulation performance change as R_2 decreases. Fig. 8 shows how the crossover frequency and phase margin vary as a function of this resistance. It can be clearly observed that, as the dynamic

resistance gets lower than the maximum values, the phase margin increases. As a consequence, the response is stable for every operating point. Concerning the dynamics, the response slows down when the resistance decreases. However, the crossover frequency variation is less important than for the PV1 voltage regulation, and the PV2 voltage response is fast enough for every operating point.

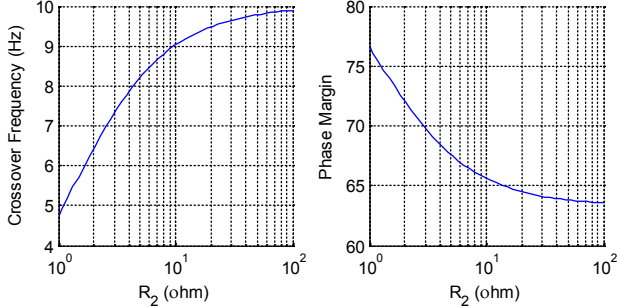


Fig. 8. Crossover frequency and phase margin as a function of R_2 for the PV2 voltage regulation.

V. SIMULATION RESULTS

The TIBuck converter, presented in Fig. 1(c) and Table I, and the two PV arrays, shown in Table II, were modeled using the software PSIM.

The PV1 voltage regulation, scheme as shown in Fig. 3, was first validated. For this purpose, the TIBuck output is modeled as a constant voltage source with $V_o=40$ V. In Fig. 9, the voltage response is represented for an irradiance of 1000 W/m² and an array temperature of 25°C . It consists in 4 V downward steps of the PV1 voltage reference from 64 V, close to the open-circuit voltage ($V_{oc1}=64.8$ V), to 48 V, below the MPP voltage ($V_{MPP1}=51.9$ V). Voltages v_1 , $v_{1,ref}$, v_2 , and v_o are shown in the first graph, duty cycle D is plotted in the second graph, and PV powers P_1 and P_2 are represented in the third graph. It can be observed how PV1 voltage response becomes faster and less damped as PV1 voltage decreases, due to the dynamic resistance R_1 increase. In any case, the rise time and overshoot are adequate for every operating point.

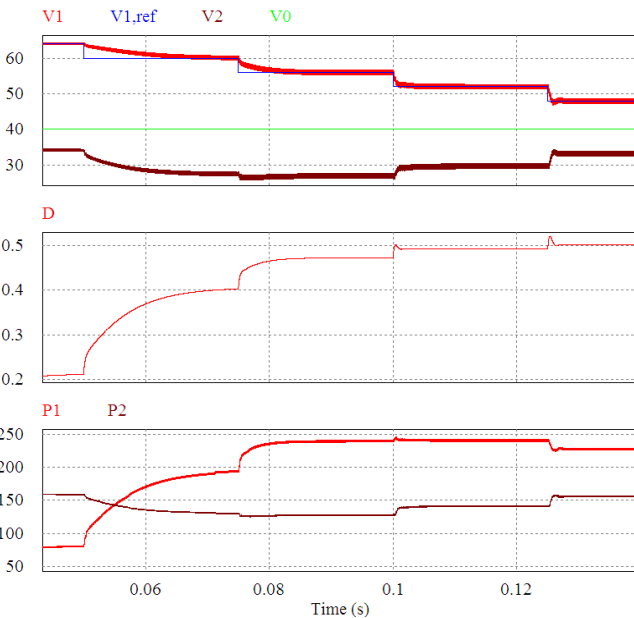


Fig. 9. Simulation of the PV1 voltage control.

The regulation of the two PV voltages at the same time was validated in a second simulation. In this case, the output capacitor C_o and the inverter are replaced by a controlled voltage source, whose value is obtained as $v_o=G_{v_o,cl}v_{o,ref}$. In order to regulate PV1 and PV2 voltages, the controls of Fig. 3 and Fig. 7 were applied. In Fig. 10, the voltage response is represented for an irradiance of 1000 W/m² and an array temperature of 25°C . For PV1 voltage, the same downward steps as in Fig. 9 are applied (note that the time scale is different). For PV2 voltage, 2.5 V reference downward steps are set from 43.5 V, close to the open-circuit voltage ($V_{oc2}=44$ V), to 33.5 V, below the MPP voltage ($V_{MPP2}=36$ V). The steps are applied at the same time to both voltages, as it would be done by the MPPT algorithm. Voltages v_1 , $v_{1,ref}$, v_2 , $v_{2,ref}$, v_o , and $v_{o,ref}$, duty cycle D , and PV powers P_1 and P_2 are shown in the figure. As it can be observed, the response becomes faster for both voltages when the dynamic resistances R_1 and R_2 increase, as it was predicted. The figure also shows that the PV2 voltage response is affected by the $v_{1,ref}$ change, which is a disturbance for the control, while the PV1 voltage response is hardly affected by the $v_{2,ref}$ and consequent v_o changes. In any case, a correct regulation of both PV voltages is obtained, which makes the control suitable to maximize the PV power of two PV arrays at the same time.

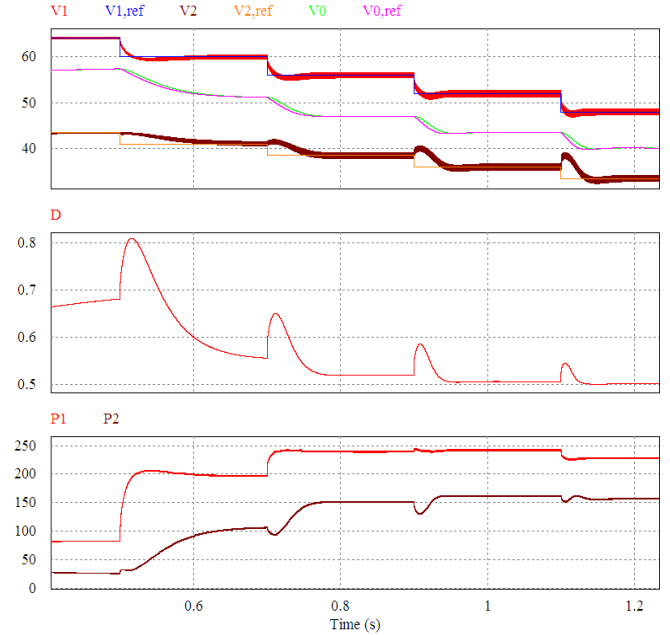


Fig. 10. Simulation of the PV1 and PV2 voltage controls.

VI. EXPERIMENTAL RESULTS

The small-signal model and the voltage regulations are validated in this section by means of experimental results. For this purpose, a prototype of the TIBuck converter, presented in Fig. 1(c) and Table I, was built. During the tests, its first input was attached to three series-connected polycrystalline modules while its second input was attached to two series-connected monocrystalline modules, features shown in Table II. The TIBuck output was connected to both an electrolytic capacitor and the electronic DC load LD300 (TTi), what made it possible to emulate the second stage converter control. The system control was implemented by using a dSPACE DS1104 R&D controller board with ControlDesk and Matlab/Simulink

software packages. The experimental setup is shown in Fig. 11, where the PV modules were facing north with a tilt angle of 24 degrees, optimum orientation for grid-connected PV systems in Sydney (Australia).

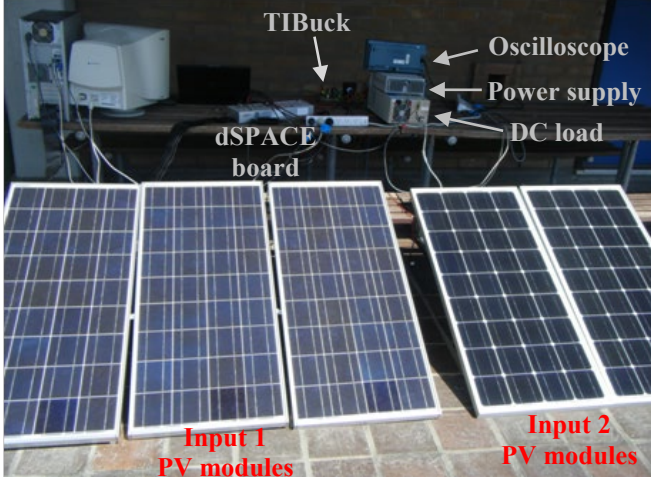


Fig. 11. Experimental setup.

The transfer function for the control of the PV1 voltage by means of the duty cycle, G_{v1-d} , theoretical expression given by (21), was experimentally obtained. For a sunny day, a small-signal duty cycle was introduced around $D=0.5$, leading to $I_1=I_2$ [see (4) and (5)]. The DC output voltage V_0 was adjusted in order to set the desired operating point, i.e. Constant Current (CC) region, Maximum Power Point (MPP) and Constant Voltage (CV) region. For each operating point, a frequency range is swept and the small-signal response is measured. High resolution oscilloscope PicoScope 4424 served to obtain the data, measuring the duty cycle d , PV voltages v_1 and v_2 , and PV current i_1 . From d and v_1 , the magnitude (dB) and phase for the bode plot were obtained. Then, from v_1 and i_1 , the operating dynamic resistance R_1 was calculated. The dynamic resistance R_2 was obtained in the same way but by means of an estimation of the PV current i_2 . By using (7) and (8), the small-signal value of i_2 can be estimated from measured variables as

$$\hat{i}_2 = \hat{i}_1 + C_2 \cdot s \cdot \hat{v}_2 - C_1 \cdot s \cdot \hat{v}_1 - (I_L / D) \cdot \hat{d}. \quad (35)$$

The experimental and theoretical bode plots of G_{v1-d} are represented in Fig. 12 for three different operating points: CC region ($R_1=38 \Omega$, $R_2=20 \Omega$), MPP ($R_1=11 \Omega$, $R_2=5 \Omega$) and CV region ($R_1=3 \Omega$, $R_2=2.4 \Omega$). The lines represent the theoretical response and the points represent the experimental values. As it can be observed, the experimental points match the model developed in section IV.A.

Once the model was validated, the PV1 voltage regulation was tested. PV1 voltage, PV2 voltage, output voltage and PV1 current are depicted in Fig. 13 for steps of the PV1 voltage reference. At the moment of this test, the conditions for the PV1 array were $V_{oc1}=59.2 \text{ V}$ and $V_{MPP1}=45.7 \text{ V}$, while V_0 was maintained equal to 35 V so that the PV2 array operated in the CC region with high R_2 values. It can be observed that the PV1 voltage regulation speeds up when reducing the PV1 voltage due to the R_1 increase, as predicted by the theoretical analysis (see Fig. 6) and by the simulation results (see Fig. 9). In any case, this figure corroborates that the PV1 voltage response is

fast enough and stable for the whole operating range of R_1 together with high values of R_2 (note that high resistance values are more problematic concerning stability).

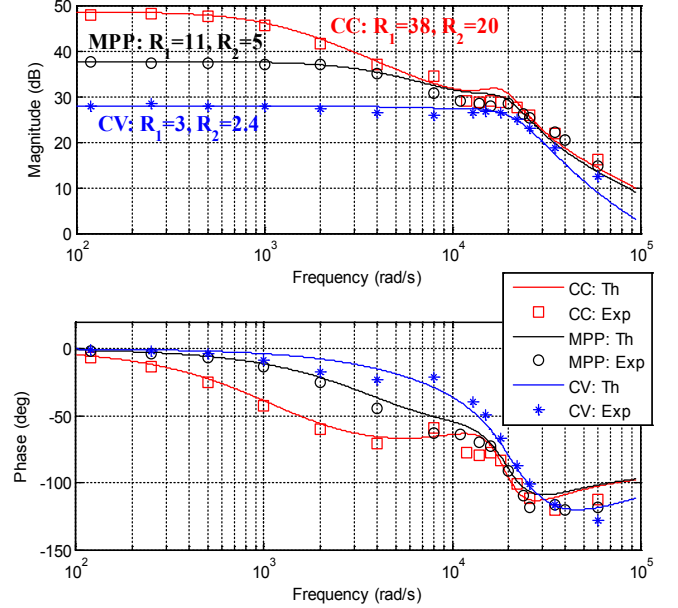


Fig. 12. Experimental and theoretical bode plots of $-G_{v1-d}$.

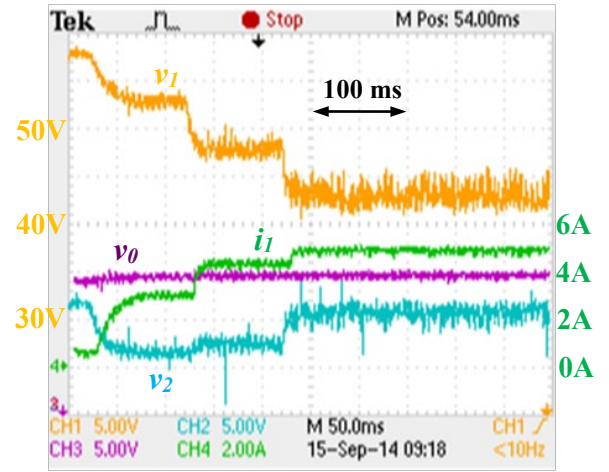


Fig. 13. Experimental results for the PV1 voltage control.

The regulation of the two PV voltages at the same time was validated in another test. In this case, the DC load controlled the output voltage according to an external reference $v_o = G_{vo,cl} v_{o,ref}$, where $v_{o,ref}$ comes from the C_{v2} controller (see Fig. 7). PV1 voltage, PV2 voltage, output voltage and PV1 current are depicted in Fig. 14 for steps of the PV1 and PV2 voltage reference, which are applied at the same time, as it would be done by the MPPT algorithm. At the moment of this test, the conditions were $V_{oc1}=59.8 \text{ V}$ and $V_{MPP1}=46.3 \text{ V}$ for the PV1 array, and $V_{oc2}=38.6 \text{ V}$ and $V_{MPP2}=31.0 \text{ V}$ for the PV2 array. As it can be observed in the figure, both v_1 and v_2 responses become faster as the dynamic resistances increase. The figure also shows how the PV2 voltage regulation is affected by the changes in the PV1 voltage reference whereas the PV1 voltage regulation is not perturbed by the PV2 voltage control. These results are thus in agreement with the previous analysis and demonstrate the ability of the converter to quickly

follow the MPPT voltage, even for such a negative situation with deep and abrupt voltage variations. As a result, the proposed control is suitable to maximize the PV power of two PV arrays at the same time.

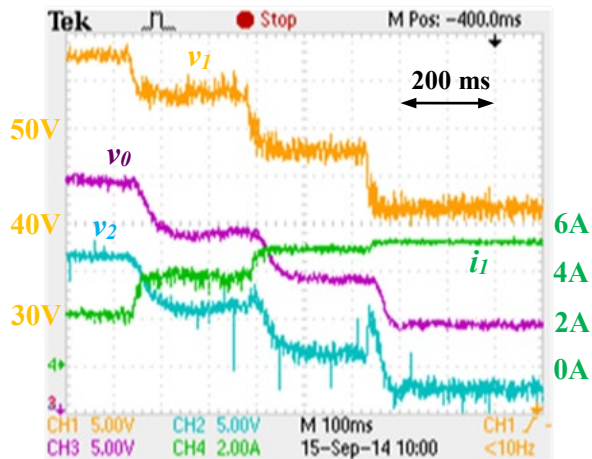


Fig. 14. Experimental results for the PV1 and PV2 voltage controls.

VII. MULTIPLE-INPUT BUCK CONVERTER

Using the two-input buck converter for MPPT of two PV strings has been proposed in this paper. Following the same philosophy, this converter can be extended to form a multiple-input buck converter [41], as shown in Fig. 15. This converter maintains the same favorable performance in terms of conversion efficiency, integration, cost and voltage stress in the switches. Furthermore, when its output is connected to another converter, it makes it possible to perform n MPPT algorithms with $n-1$ active switches. On the other hand, the restrictions are that the voltage v_n must be lower than all other PV voltages, and that the active switches must block negative currents. The latter can be easily achieved by using an IGBT transistor or by adding a diode in series with the MOSFET transistor, but the first solution is preferred for efficiency.

Concerning the control of the multiple PV voltages, it seems appropriate that each active switch regulates its corresponding PV voltage, being able to achieve fast dynamic response. For its part, the voltage of the n^{th} PV array would be controlled by means of the output voltage, similarly to the TIBuck converter. As a result, the voltage responses of v_1, v_2, \dots, v_{n-1} cannot be decoupled and the control study becomes more complicated. In any case, the control and in-depth analysis of the multiple-input buck converter has not been carried out but is part of the authors' future work.

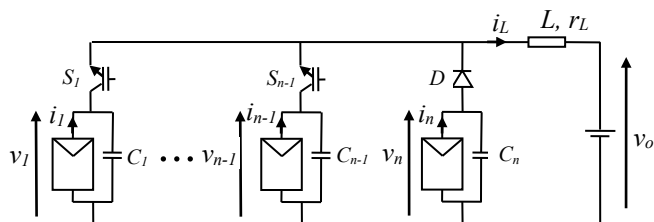


Fig. 15. Multiple-input buck converter.

VIII. CONCLUSIONS

The two-input buck converter shows an interesting solution for the first stage of PV systems thanks to its simplicity, reliability and two-MPPT capability with only one active switch. However, the presence of two nonlinear PV arrays together with the nonlinear converter makes the voltage control design a delicate task.

A control scheme for regulating the two input voltages is first presented in this paper. Then, a system small-signal modeling which accounts for the nonlinear characteristics of the converter and the two PV arrays is derived. Thanks to the derived model, the two controllers are designed and the effect of the dynamic resistances on the control performance is evaluated. It is shown that the dynamic response becomes slower and more damped as the operating point moves towards the constant voltage region, and that stability is ensured for every situation. Simulation and experimental results validated the analysis and showed that the proposed voltage regulation is adequate to perform MPPT of two arrays at the same time.

REFERENCES

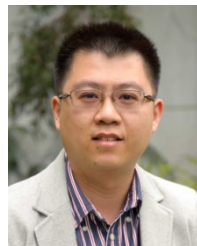
- [1] REN21 Renewable Energy Policy Network for the 21st Century, "Renewables Global Status Report 2014".
- [2] X. Xiong, C. K. Tse, and X. Ruan, "Bifurcation analysis of stand-alone photovoltaic-battery hybrid power system," *IEEE Trans. Circuits Syst. I, Reg Papers*, vol. 60, no. 5, pp. 1354-1365, 2013.
- [3] G.-S. Seo, J.-W. Shin, B.-H. Cho, and K.-C. Lee, "Digitally controlled current sensorless photovoltaic micro-converter for DC distribution," *IEEE Trans. Ind. Informat.*, vol. 10, no. 1, pp. 117-126, 2014.
- [4] E. Mamarelis, G. Petrone, and G. Spagnuolo, "An hybrid digital-analog sliding mode controller for photovoltaic applications," *IEEE Trans. Ind. Informat.*, vol. 9, no. 2, pp. 1094-1103, 2013.
- [5] Y.-J. Wang, and P.-C. Hsu, "Analytical modelling of partial shading and different orientation of photovoltaic modules," *IET Renew. Power Gen.*, vol. 4, no. 3, pp. 272-282, 2010.
- [6] A. Maki, and S. Valkealahti, "Power losses in long string and parallel-connected short strings of series-connected silicon-based photovoltaic modules due to partial shading conditions," *IEEE Trans. Energy Convers.*, vol. 27, no. 1, pp. 173-183, 2012.
- [7] M. Z. S. El-Dein, M. Kazerani, and M. M. A. Salama, "An optimal total cross tied interconnection for reducing mismatch losses in photovoltaic arrays," *IEEE Trans. Sustain. Energy*, vol. 4, no. 1, pp. 99-107, 2013.
- [8] M. Boztepe, F. Guinjoan, G. Velasco-Quesada, S. Silvestre, A. Chouder, and E. Karatepe, "Global MPPT scheme for photovoltaic string inverters based on restrictive voltage window search algorithm," *IEEE Trans. Ind. Electron.*, vol. 61, no. 7, pp. 3302-3012, 2014.
- [9] J. D. Bastidas-Rodriguez, E. Franco, G. Petrone, C. A. Ramos-Paja, G. Spagnuolo, "Maximum power point tracking architectures for photovoltaic systems in mismatching conditions: a review," *IET Power Electron.*, vol. 7, no. 6, pp. 1396-1413, 2014.
- [10] H. Patel, and V. Agarwal, "Maximum power point tracking scheme for PV systems operating under partially shaded conditions," *IEEE Trans. Ind. Electron.*, vol. 55, no. 4, pp. 1689-1698, 2008.
- [11] K. S. Tey, and S. Mekhilef, "Modified incremental conductance algorithm for photovoltaic system under partial shading conditions and load variation," *IEEE Trans. Ind. Electron.*, vol. 61, no. 10, pp. 5384-5392, 2014.
- [12] G. Velasco-Quesada, F. Guinjoan-Gispert, R. Pique-Lopez, M. Roman-Lumbreras, and A. Conesa-Roca, "Electrical PV array reconfiguration strategy for energy extraction improvement in grid-connected PV systems," *IEEE Trans. Ind. Electron.*, vol. 56, no. 11, pp. 4319-4331, 2009.
- [13] N. Femia, G. Lisi, G. Petrone, G. Spagnuolo, and M. Vitelli, "Distributed maximum power point tracking of photovoltaic arrays: novel approach and system analysis," *IEEE Trans. Ind. Electron.*, vol. 55, no. 7, pp. 2610-2621, 2008.
- [14] P. Tsao, S. Sarhan, and I. Jorio, "Distributed max power point tracking for photovoltaic arrays," in *IEEE Photovoltaic Specialists Conference (PVSC)*, pp. 2293-2298, 2009.

- [15] Y.-C. Chang, C.-L. Kuo, K.-H. Sun, and T.-C. Li, "Development and operational control of two-string maximum power point trackers in DC distribution systems," *IEEE Trans. Power Electron.*, vol. 28, no. 4, pp. 1852–1861, 2013.
- [16] M. J. V. Vazquez, J. M. A. Marquez, and F. S. Manzano, "A methodology for optimizing stand-alone PV-system size using parallel-connected DC/DC converters," *IEEE Trans. Ind. Electron.*, vol. 55, no. 7, pp. 2664–2673, 2008.
- [17] S. V. Dhople, J. L. Ehlmann, A. Davoudi, and P. L. Chapman, "Multiple-input boost converter to minimize power losses due to partial shading in photovoltaic modules," in *IEEE Energy Conversion Congress and Exposition (ECCE)*, pp. 2633–2636, 2010.
- [18] F. Pulvirenti, A. La Scala, D. Ragonese, K. D'Souza, G. M. Tina, and S. Pennisi, "4-phase interleaved boost converter with IC controller for distributed photovoltaic systems," *IEEE Trans. Circuits Syst. I, Reg. Papers*, vol. 60, no. 11, pp. 3090–3102, 2013.
- [19] Y. M. Chen, Y. C. Liu, and S. H. Lin, "Double-input PWM DC-DC converter for high-/low- voltage sources," *IEEE Trans. Ind. Electron.*, vol. 53, no. 5, pp. 1538–1544, 2006.
- [20] C.-T. Pan, C.-F. Chuang, and C.-C. Chu, "A novel transformerless interleaved high step-down conversion ratio DC-DC converter with low switch voltage stress," *IEEE Trans. Ind. Electron.*, vol. 61, no. 10, pp. 5290–5299, 2014.
- [21] Y.-C. Liu, and Y.-M. Chen, "A systematic approach to synthesizing multi-input DC-DC converters," *IEEE Trans. Power Electron.*, vol. 24, no. 1, pp. 116–127, 2009.
- [22] X. Sun, Y. Zhou, W. Wang, B. Wang, and Z. Zhang, "Alternative source-port-tolerant series-connected double-input DC-DC converter," *IEEE Trans. Power Electron.*, vol. 30, no. 5, pp. 2733–2742, 2015.
- [23] R.-J. Wai, C.-Y. Lin, and B.-H. Chen, "High-efficiency DC-DC converter with two input power sources," *IEEE Trans. Power Electron.*, vol. 27, no. 4, pp. 1862–1875, 2012.
- [24] L. D. Salazar, and J. R. Urra, "A novel three ports power conditioner for renewable electricity generators," in *IEEE Industrial Electronics Society Conference (IECON)*, pp. 1131–1136, 2011.
- [25] A. Khaligh, J. Cao, and Y.-J. Lee, "A multiple-input DC-DC converter topology," *IEEE Trans. Power Electron.*, vol. 24, no. 3, pp. 862–868, 2009.
- [26] R.-J. Wai, and L.-S. Hong, "High-efficiency dual-input converter with high-voltage gain and internal charge function," *IET Power Electron.*, vol. 7, no. 2, pp. 299–315, 2014.
- [27] J. Sebastian, P. Villegas, F. Nuno, and M. Hernando, "High-efficiency and wide-bandwidth performance obtainable from a two-input buck converter," *IEEE Trans. Power Electron.*, vol. 13, no. 4, pp. 706–717, 1998.
- [28] A. Urtasun, P. Sanchis, and L. Marroyo, "Adaptive voltage control of the dc/dc boost stage in PV converters with small input capacitors," *IEEE Trans. Power Electron.*, vol. 28, no. 11, pp. 5038–5048, 2013.
- [29] M. G. Villalva, T. G. de Siqueira, and E. Ruppert, "Voltage regulation of photovoltaic arrays: Small-signal analysis and control design," *IET Power Electron.*, vol. 3, no. 6, pp. 869–880, 2010.
- [30] L. Nousiainen, J. Pukko, A. Maki, T. Messo, J. Huusari, J. Jokipii, J. Viinamaki, D. T. Lobera, S. Valkealahti, and T. Suntion, "Photovoltaic generator as an input source for power electronic converters," *IEEE Trans. Power Electron.*, vol. 28, no. 6, pp. 3028–3038, 2013.
- [31] W. Xiao, W. G. Dunford, P. R. Palmer, and A. Capel, "Regulation of photovoltaic voltage," *IEEE Trans. Ind. Electron.*, vol. 54, no. 3, pp. 1365–1374, 2007.
- [32] A. Urtasun, E. L. Barrios, P. Sanchis, and L. Marroyo, "Frequency-based energy management for stand-alone systems with distributed battery storage," *IEEE Trans. Power Electron.*, vol. 30, no. 9, pp. 4794–4808, 2015.
- [33] C. R. Sullivan, J. J. Awerbuch, and A. M. Latham, "Decrease in photovoltaic power output from ripple: simple general calculation and the effect of partial shading," *IEEE Trans. Power Electron.*, vol. 2, no. 2, pp. 740–747, 2013.
- [34] M. A. Gomes de Brito, L. Galotto Jr., L. P. Sampaio, G. de Azevedo e Melo, and C. A. Canesin, "Evaluation of the main MPPT techniques for photovoltaic applications," *IEEE Trans. Ind. Electron.*, vol. 60, no. 3, pp. 1156–1167, 2013.
- [35] F. Paz, and M. Ordóñez, "Zero oscillation and irradiance slope tracking for photovoltaic MPPT," *IEEE Trans. Ind. Electron.*, vol. 61, no. 11, pp. 6138–6147, 2014.
- [36] A. Urtasun, P. Sanchis, and L. Marroyo, "Limiting the power generated by a photovoltaic system," in *IEEE Multi-Conference on Systems, Signals and Devices (SSD)*, pp. 1–6, 2013.
- [37] R. González, J. López, P. Sanchis, and L. Marroyo, "Transformerless inverter for single-phase photovoltaic systems," *IEEE Trans. Power Electron.*, vol. 22, no. 2, pp. 693–697, 2007.
- [38] Z. Ye, P. K. Jain, and P. C. Sen, "A full-bridge resonant inverter with modified phase-shift modulation for high-frequency AC power distribution systems," *IEEE Trans. Ind. Electron.*, vol. 54, no. 5, pp. 2831–2845, 2007.
- [39] A. Safari and S. Mekhilef, "Simulation and hardware implementation of incremental conductance MPPT with direct control method using Cuk converter," *IEEE Trans. Ind. Electron.*, vol. 58, no. 4, pp. 1154–1161, 2011.
- [40] T. Messo, J. Jokipii, J. Puukko, and T. Suntion, "Determining the value of dc-link capacitance to ensure stable operation of a three-phase photovoltaic inverter," *IEEE Trans. Power Electron.*, vol. 29, no. 2, pp. 665–673, 2014.
- [41] M. Rodríguez, P. Fernandez-Miaja, A. Rodríguez, and J. Sebastián, "A multiple-input digitally controlled buck converter for envelope tracking applications in radiofrequency power amplifiers," *IEEE Trans. Power Electron.*, vol. 25, no. 2, pp. 369–381, 2010.



Andoni Urtasun (S'11) was born in Pamplona, Spain, in 1987. He received the M.Sc. degree in electrical engineering from the Public University of Navarre (UPNa), Pamplona, Spain, and from the Institut National Polytechnique de Toulouse, Toulouse, France, both in 2010, and the Ph.D. degree in electrical engineering from the UPNa in 2015.

In 2010, he joined the Electrical Engineering, Power Electronics and Renewable Energy research group, UPNa, where he is currently Assistant Professor. During 2014, he was visiting scholar in The University of Sydney, Australia. His research interests include renewable energy systems and control of power electronic converters.



Dylan Dah-Chuan Lu (S'00 – M'04 – SM'09) received his B.Eng. (Hons.) and Ph.D. degrees in Electronic and Information Engineering from The Hong Kong Polytechnic University, Hong Kong in 1999 and 2004 respectively.

In 2003, he joined PowerLab Ltd. as a Senior Design Engineer. His major responsibilities included project development and management, circuit design, and contribution of research in power electronics. In 2006, he joined the School of Electrical and Information Engineering, The University of Sydney, Australia, where he is currently a Senior Lecturer. From July 2013 to December 2013, he was with the University of Hong Kong as a visiting Associate Professor. He is the author and co-author of over 120 papers in the areas of power electronics and engineering education. He has two patents on efficient power conversion. His current research interests include power electronics circuits and control for efficient power conversion, lighting, renewable electrical energy systems, microgrids, motor drive and power quality improvement, and engineering education.

Dr. Lu is a member of the Institute of Engineers Australia. He presently serves as an Associate Editor of the *IET Renewable Power Generation* and the *International Journal of Electronics*. He also serves as a Guest Editor of the *IEEE Transactions on Industrial Electronics*; special issue on Power Converters, Control and Energy Management for Distributed Generation in 2014.